Journal of Molecular Modeling (2023) 29:4
https://doi.org/10.1007/s00894-022-05402-6

ORIGINAL PAPER

Efficient and tunable enhancement of NLO performance for indaceno-based donor moiety in A-π-D-π-D-π-A type first DSSC design by end-capped acceptors

Abrar U. Hassan[1] · Sajjad H. Sumrra[1] · Ghulam Mustafa[1] · Muhammad F. Nazar[2] · Muhammad N. Zafar[1]

Received: 24 June 2022 / Accepted: 29 November 2022 / Published online: 9 December 2022

Abstract

Background The organic dyes with non-fullerene acceptors (NFAs) have aided in the creation of competitive organic solar cells (OSCs) with long-term sustainability. A series of NFA dyes (**IDIC-R1**–**IDIC-R9**) have been designed by varying the end-capped fluorinated moieties (**PD1–PD6**) at indaceno (**IDIC**) core.

Methods All the calculations were performed by density functional theory (DFT) and time-dependent DFT (TD-DFT)–based approaches. All the geometries were optimized at B3LYP/6-31G + (d,p) of DFT level at their ground state energies. Out of several density functionals, the CAM-B3LYP with 6-31G + (d,p) basis sets was selected after a benchmark study to carry out further calculations. All the dyes had their bandgaps in 0.11–3.12 eV while their starting reference dye had a bandgap value of 2.01 eV.

Results Their ionization potential (IP) implied that these dyes have strong tendency to lose electrons. The λ_{max} of the dyes was slightly redshifted from the **IDIC** (476 nm) and **IDIC-R** (479 nm) when changing solvent polarity from methanol to DCM and then chloroforms. The natural bond orbital (NBO) analysis showed the (S63)LP → (C61-C62)π* with highest stabilization energy. Their electron injection analysis showed that these dyes can be a good anode material against the aluminum and gold electrodes. The intramolecular charge transfer (ICT) process and stability of the dyes were investigated using frontier molecular orbital (FMO) and natural bond orbital (NBO) analysis.

Conclusion Among all dyes, **IDIC-R8** has the highest linear polarizability and second-order hyperpolarizability (β_{total}). All the dyes demonstrated promising non-linear optical (NLO) properties due to their low charge transfer barriers. Scientists would be able to exploit these properties to identify the best NLO materials for existing applications.

Keywords ICT · NLO · Non-Fullerene · NBO · UV–Vis

Introduction

The organic dyes are the most promising groups for optical chemistry [1] with excellent photo-physical properties inside the near-infrared region (NIR) [2] with intramolecular charge transfer (ICT) [3] features. Changing a multifunctional component in the synthesis of fluorescent organic dyes is an excellent way to adjust their absorption and/or emission wavelengths [4] for dye sensitized solar cell (DSSC) applications [5]. The organic solar cells (OSCs) [6] as optical probes are also useful in photovoltaic (PV) [7] and optical applications [8]. The materials with good non-linear optical (NLO) properties have received interest due to their potential use in high-tech applications [9] by having fast response time [10]. They have also been extensively customized for optical storage systems and as photodetector switches [11]. A comparative analysis of organic and inorganic NLO materials reveals that organic systems have various benefits over inorganic materials including a fast response time, high structural flexibility, high processing effectiveness, and a high non-linear polarization rate [12].

✉ Abrar U. Hassan
hassanabrar2016@gmail.com

✉ Sajjad H. Sumrra
sajjadchemist@uog.edu.pk

[1] Department of Chemistry, University of Gujrat, Gujrat 50700, Pakistan

[2] Department of Chemistry, Division of Science and Technology, University of Education, Multan Campus, Lahore 60700, Pakistan

The organic dyes with a high interconnecting electron density as well as electronic density may be desirable features for second- and third-order NLO materials [13]. Powerful electron-withdrawing moieties have also been added to the ends of A-D-A-D-A type dyes to provide highly efficient non-fullerene acceptors (NFAs) that have exhibited a variety of PV features [14]. With enhanced DSSC capabilities, the effects of various supplementary donor (D) units before and after binding upon the photogenerated electrons have been investigated [15]. Changing the chemical structure to produce major NLO response is thus an intelligent method [16] in which highly interconnected electron density may be a superior requirement for its tunable response [17]. The D and acceptor (A) moieties are also responsible for the required ground state charge balance to tune the NLO performance [18].

The NFAs have attracted the curiosity of many researchers to their enhanced PV features [19]. In order to get around the limits of fullerene-based dyes, researchers are currently working to create inexpensive NFAs for OSCs in PV devices [20]. They have surpassed their fullerene counterparts in terms of light absorption and D-A combination variety [21]. Theoretical studies on these A units and thiophene bridging units are the focus of the current investigation. The proposed molecules' various optoelectronic properties were computed which had just been published with promising findings. These A units displayed broad spectra, a smaller band gap, and the greatest open-circuit voltage values, according to the results. They have widely been used as a D units to pair with different A units to create a range of D-A conjugated materials, which have emerged one of the key categories for OSCs [22]. A wide variety of NFAs have now been studied for their electro- and PV properties over the last 10 years due to its notable electron carrier possibilities.

The outcomes of the NLO attributes investigation with the title NFA dyes have not been communicated still. To bridge this research gap, the theoretical simulations based on density functional theory (DFT) were used to examine NLO characteristics. Predicated on these interesting aspects of cross-linked NF-based molecules, we chose NFA dyes in this study to investigate their NLO capabilities theoretically. The dimalononitrile-based moiety of 2,2′-((4-heptyl-4,9,9-trihexyl-4,9-dihydro-s-indaceno[1,2-b:5,6-b′]dithiophene-2,7-diyl)bis(methanylylidene)bis(3-oxo-2,3-dihydro-1H-indene-1-yl-2-ylidene)dimalononitrile (**IDIC**) [23] is a promising building component for the development of organic devices. Different NFA units have been developed by combining them with conjugated π-spacers to design NFA-based **IDIC-R1–IDIC-R9** new dyes. Before designing these dyes, the starting material (IDIC) was modified structurally to design a reference dye **IDIC-R** for the sake of its compact molecular packing with improved derive parameters related to solar cells (Fig. 1). Because it elucidates the effects of the **D**, multiple A units, and π-spacers in NFA dyes, this study is crucial for estimating NLO implementation. Natural bond orbital (NBO) analysis, global reactivity parameters (GRPs), frontier molecular orbitals (FMOs), densities of states (DOSs), and ultraviolet–visible (UV–Vis) absorption spectra were derived using DFT and TD-DFT predictions for NLO features. The NFAs are thought to have a significant influence on the non-linear optical field. Because it elucidates the effects of the D, multiple A units, and π-spacers in NFA dyes, this study is crucial for estimating their NLO implementation.

Methodology

The current investigation was carried out by operating the Gaussian 09 package [24]. All the molecular geometries of the dyes were optimized at Becke, 3-parameter, Lee–Yang–Parr (B3LYP) density functional (DF) with 6-31G + (d,p) basis sets. All the optimizations were performed at 300 atm pressure with 2.0 psi pressure which were adjusted by including in the basis sets "functional/basis set freq temperature = 300.0 pressure = 2.0."

Several long-range and range-separated DFs were applied on the output files of optimized geometries to benchmark their absorbance maxima (λ_{max}) [25] of new dyes. Out of this benchmarking, the DF of CAM-B3LYP with 6-31G + (d,p) basis gave the closest λ_{max} and was selected for further studies. The parameters for FMO, NBO, density of state (DOS), projected UV–Vis absorbance [26], and NLO characteristics of NFA dyes with a very A-π-D-π-D-π-A architecture were determined. The bandgap was calculated using an FMO analysis, which enabled the lowest amount of energy necessary for the transition from their highest occupied molecular orbital (HOMO) to lowest unoccupied molecular orbitals (LUMO) to be computed. Their hyper-conjugative connections were analyzed by utilizing their NBO analysis. The DOS calculations were used to calculate the dispersion of energy states between their FMOs. The UV–Vis absorption spectra were obtained to investigate their ICT, dipole moment (μ_{nor}), and linear polarizability including first hyperpolarizability (α) and second hyperpolarizability (β_{tot}). The findings were obtained from output files applying the GaussView [27], Avogadro [28], and Chemcraft [29] software packages.

The energies of LUMOs (E_{LUMO}) and HOMOs (E_{HOMO}) have been used to illustrate reactivity and stability for studying the GRP [30] such as electron affinity (EA), electrophilicity index (ω), ionization potential (IP), chemical potential (μ), electronegativity (χ), hardness (η), and softness (σ). By using Koopmans' theorem, the formulae below are used to calculate different parameters.

$$\mathbf{IP} = -E_{HOMO} \quad (1)$$

$$\mathbf{EA} = -E_{LUMO} \quad (2)$$

$$\chi = \left(\frac{\mathbf{IP} + \mathbf{EA}}{2}\right) \tag{3}$$

$$\eta = \frac{1}{2}(E_{\mathrm{LUMO}} - E_{\mathrm{HOMO}}) \tag{4}$$

$$\mu = -\left(\frac{\mathbf{IE} + \mathbf{EA}}{2}\right) \tag{5}$$

$$\sigma = \frac{1}{2\eta} \tag{6}$$

When a single-molecule system acquires an additional surface charge density from its surroundings, it monitors energy constancy, as defined by Parr [31]. It is a feature of reactivity that allows for quantitative classification of

$$\omega = \left(\frac{\mu^2}{2\eta}\right) \tag{7}$$

Light harvesting efficiency (LHE) is also another crucial segment that influences optical performance. The charge transfer (CT) sensitivity of dyes with a high LHE content is greatest. The LHE of dyes can be computed using the formula (8).

$$LHE = 1 - 10^{-f} \tag{8}$$

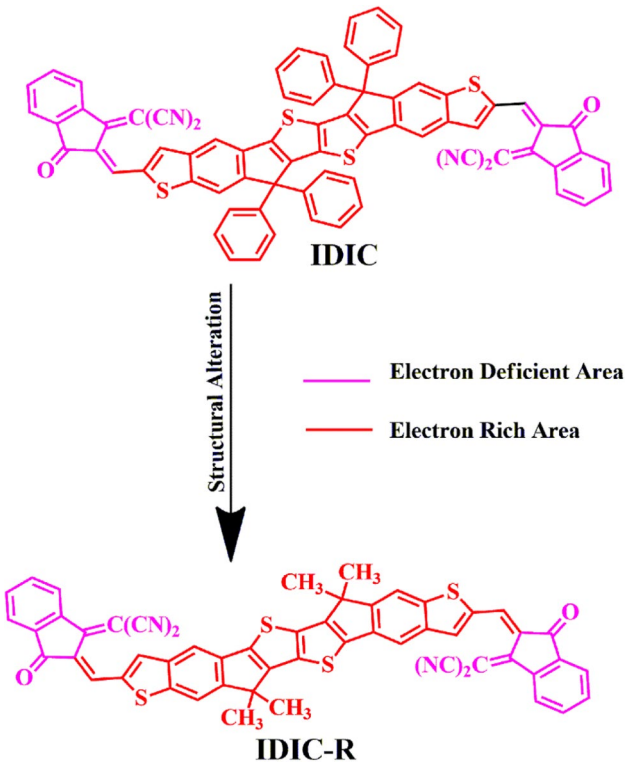

Fig. 1 Structural alteration of dye **IDIC** to create the reference dye **IDIC-R**

The calculation below is commonly used to calculate open circuit voltage (V_{oc}), an essential parameter for measuring the cost-efficiency of semiconductor applications.

$$V_{oc} = \frac{1}{e}\left(\left[E_{\mathrm{HOMO(D)}} - E_{\mathrm{LUMO(A)}}\right]\right) - 0.03 \tag{9}$$

Equations (10) and (11) were used to compute the NLO responses of dyes as $\alpha\ \beta_{tot}$ by using their tensors [32] of polarizability.

$$< \alpha >= 1/3(\alpha_{xx} + \alpha_{yy} + \alpha_{zz}) \tag{10}$$

$$\beta_{tot} = \left[(\beta_{xxx} + \beta_{xyy} + \beta_{xzz})^2 + (\beta_{yyy} + \beta_{xxy} + \beta_{yzz})^2 + (\beta_{zzz} + \beta_{xxz} + \beta_{yyz})^2\right]^{1/2} \tag{11}$$

Results and discussion

The present research has focused on NFA-based organic dyes for DSSCs and their other related properties such as GRP NLO analysis. With first D (D1) which was 4-methyl-3a,4-dihydrocyclopenta[b]indole (**MDI**), we utilized the 2,2′-((4-heptyl-4,9,9-trihexyl-4,9-dihydro-s-indaceno[1,2-b:5,6-b′]dithiophene-2,7-diyl)bis(methanylylidene)bis(3-oxo-2,3-dihydro-1H-indene-1-yl-2-ylidene)dimalononitrile (**IDIC**) as second D (D2). It was selected due to the fact that it is a highly common PV material and also there was no illustration of such electron-rich versus electron-poor states to establish a pull–push phenomenon. Following methyl substitutions on its short axis of **IDIC**, the energy bandgap was dropped with their enhanced λ_{max} and improved NLO response. The reference dye **IDIC-R** was also projected to be with improved exciton energy production and with more controlled CT mobility.

First second and π-spacers were aromatic rings while π-spacer number 3 was 2,2′-bithiophene. The novel DSSC design with A-π-D-π-D-π-A type layout was divided into seven parts: A1, π-spacer, D1, π-spacer, D2, and π-spacer and A2.

For end-capped moieties, propanedinitrile as A units along with its various fluorinated and cynated versions were used. All the A units included (1-oxo-1H-inden-3-yl) propanedinitrile (**PD1**), (4-fluoro-1-oxo-1H-inden-3-yl) propanedinitrile (**PD2**), (4,6-difluoro-1-oxo-1H-inden-3-yl) propanedinitrile (**PD3**), 2,2′-(1*H*-indene-1,3-diyl)dipropanedinitrile (**D4**), 2,2′-(6-fluoro-1*H*-indene-1,3-diyl)dipropanedinitrile (**PD5**), and 2,2′-(4,6-difluoro-1H-indene-1,3-diyl) dipropanedinitrile (**PD6**). We used numerous long-range and range-separated DFs to replicate its experimental maximum value. The moiety **IDIC** served as a reference to benchmark different DFs, as did its newly created dyes **IDIC-R1–IDIC-R9**. In the suggested dyes, a first D moiety, second D moieties, and π-spacers were retained for building construction;

however, the A units (**PD1**–**PD6**) were substituted. In this situation, the NLO assessments, polarizability by DFT, and (iii) absorption wavelengths by TD-DFT were computed to offer understanding of how different A units functioned and how constant units influenced NLO and PV-related parameters. The first D moiety (**MDI**), second D moiety (**IDIC**), phenyl and 2,2′-bithiophene π-spacers, and A substituents (**A1**–**A6**) were kept in the dyes **IDIC-R1**–**IDIC-R9** for building purposes.

Modeling of A-π-D-π-D-π-A framework

The dyes comprising D-π-A must have their geometry optimized to achieve a stable alignment in order to have good PV potential [33]. Their structural morphologies must be screened because they are crucial in determining the μ_{nor}, efficient packing ability, as well as other PV-related characteristics. All of these dye-related factors are crucial for obtaining their NLO performances. For D-π-A style fluorescent dyes, filtering of A units is critical for achieving a good NLO performance [34]. The goal of this research was to create a new indaceno moiety–based interesting NLO switches by being structurally tailored with different π-bridges and to forecast their optoelectronic, electrical, and NLO characteristics for the newest optoelectronics. This is where and why such theoretical engineering takes place. These six π-conjugates served as the major end-capped A units, while two types of π-spacers serve as the secondary π-linkers, resulting in a total of nine dye molecules (Fig. 2).

Our proposed materials (**IDIC-R1** to **IDICR9**) were made up of three primary components: the D moieties of **IDIC** and **MDI**, first and second π-spacers as phenyl, and third π-spacer as 2,2′-bithiophene, which served as a bridging link, and A components (1-oxo-1H-inden-3-yl)propanedinitrile. All the dyes had the dihedral angles spanning 117–118.5° for C–C–C in the framework aromatic (benzene) rings. The binding angle between C–C–N bond was found to be around 106–110°.

The C–N–C bond angle of such **MDI** corner benzene ring was determined to be identical, ranging between 112 and 114°. The dihedral angles of C–C–N were calculated to be 107–111°. The geometric bond angle between C and C–N was 106–107°. In case of dye **IDIC-R1**, similar outcomes were observed for the bond angles of C1-C3-C5, C16-N14-C75, and C3-C1-C16, which were 120.23–121.33° (Fig. 3). The bond angles between the bithiophene ring atoms like C83-C81-S82 were at 121.3°. By adding large donor atomic units, the indole structure was considerably changed, but the symmetrical arrangement of the phenyl ring was unaffected. Two phenyl conjugates were used to create dyes with different acceptor atoms. All the dihedral angles of the aromatic rings were 117.65–118.09°.

FMO analysis

A FMO study may be used to evaluate the investigated dyes for their essential quantum chemical properties, such as electronic metrics, chemical stability, energy transfer qualities, and their chemical reactivity [26]. Such studies also regulate electron–hole pair, ω, chemical reactivity, and σ as a pull–push effect. All the dyes with their thermodynamic and chemical stability were inextricably linked to their difference in energy of their FMOs (bandgap = $E_{LUMO} - E_{HOMO}$) (Table 1). It can be rationalized from their bandgap values that the reference dye IDIC-R had a considerably low value than that of its starting materials **IDIC** and then the new dyes had further a reduction of their values except a few dyes.

Among all, the dye **IDIC-R7** had a bandgap value of 5.88 eV, which was greater than the bandgap of **IDIC** (3.12 eV) while dyes **IDIC-R4**, **IDIC-R5**, **IDIC-R8**, and **IDIC-R9** had lower values than the **IDIC-R** (1.11). Overall bandgap for all proposed dyes were calculated as follows: **IDIC-R7** (5.88) > **IDIC** (3.12) > **IDIC-R3** (2.42) > **IDIC-R6** (2.22) > **IDIC-R1** (1.27) > **IDIC-R2** (1.19) > **IDIC-R** (1.11) > **IDIC-R4** (1.03) > **IDIC-R5** (0.65) > **IDIC-R9** (0.65) > **IDIC-R8** (0.11). The D, A, π-spacers, and end A units are all involved in ordering the dyes, which had significantly reduced their bandgap. The reduction in bandgap observed for dyes had demonstrated how a position of a small molecule can affect the energy variations. The dyes **IDIC-R7** and **IDIC-R8** were changed because of compositional modifications and as a result bandgap values have been further decreased by adding two and one fluoro (F) on its A unit (**PD3**), where two F units were proven to be more efficient in decreasing the bandgap than one cyano (CN) unit. The analysis of FMOs in conjunction with bandgap revealed that the suggested dyes may perform ICT from D to A units through π-spacers (Fig. 4).

The D, π-spacers, and A units are found to be involved in arranging the bandgap values of these newly designed dyes. The bandgap values have been further decreased to 1.07–1.18 eV by adding two and one F unit on A units, where two F units were proven to be more efficient in decreasing the bandgap than one F unit.

The bandgap value in **IDIC-R4** reduced dramatically to 1.67 eV due to the inclusion of one F unit on the A moiety. This increase in bandgap value might be attributable to the F unit since its resonance impact is less amplified than that of the F unit. The dyes **IDIC-R2**, **IDIC-R5**, and **IDIC-R6** had lower bandgap values since F units constituted D units due to resonance phenomena. Because of the inclusion of nitro groups, bandgap measurements in **IDIC-R6** were increased about 0.22 eV. The dye **IDIC-R8** had the smallest bandgap value of all because of the clear considerable conjugation involved in phenyl rings as well as the end-capped A

segment comprising nitro units. The presence of electronegative entities (F and CN units) on A subunits can effectively lower electrostatic potential concentration from other areas of the A unit, resulting in a decrease in bandgap. With the aid of the π-spacer, the bandgap values characterize the ICT interface from D to A section, providing significant understanding into connected functional linkages of the NLO components. The contour parts of FMOs were employed to determine the transport of electrical charges. In **IDIC-R1**–**IDIC-R4**, the LUMOs for the charge density were only visible on the A unit and partially on the second π-spacer. On the first π-spacer, second D units, and A1, the electronic populations in the HOMO were discovered. Electron density from D to A or via the π-spacer was required for NLO stimulation. The dye **IDIC-R1** and **IDIC-R6** may be considered as feasible NLO contenders because of this influence.

Global reactivities

The HOMO → LUMO difference in energy (bandgap) has widely been used to compute the GRPs of newly designed compounds which include IP, EA, χ, η, ω, μ, and σ (Table 2). Understanding the association between structural system and their chemical reactivity requires the usage of conceptual

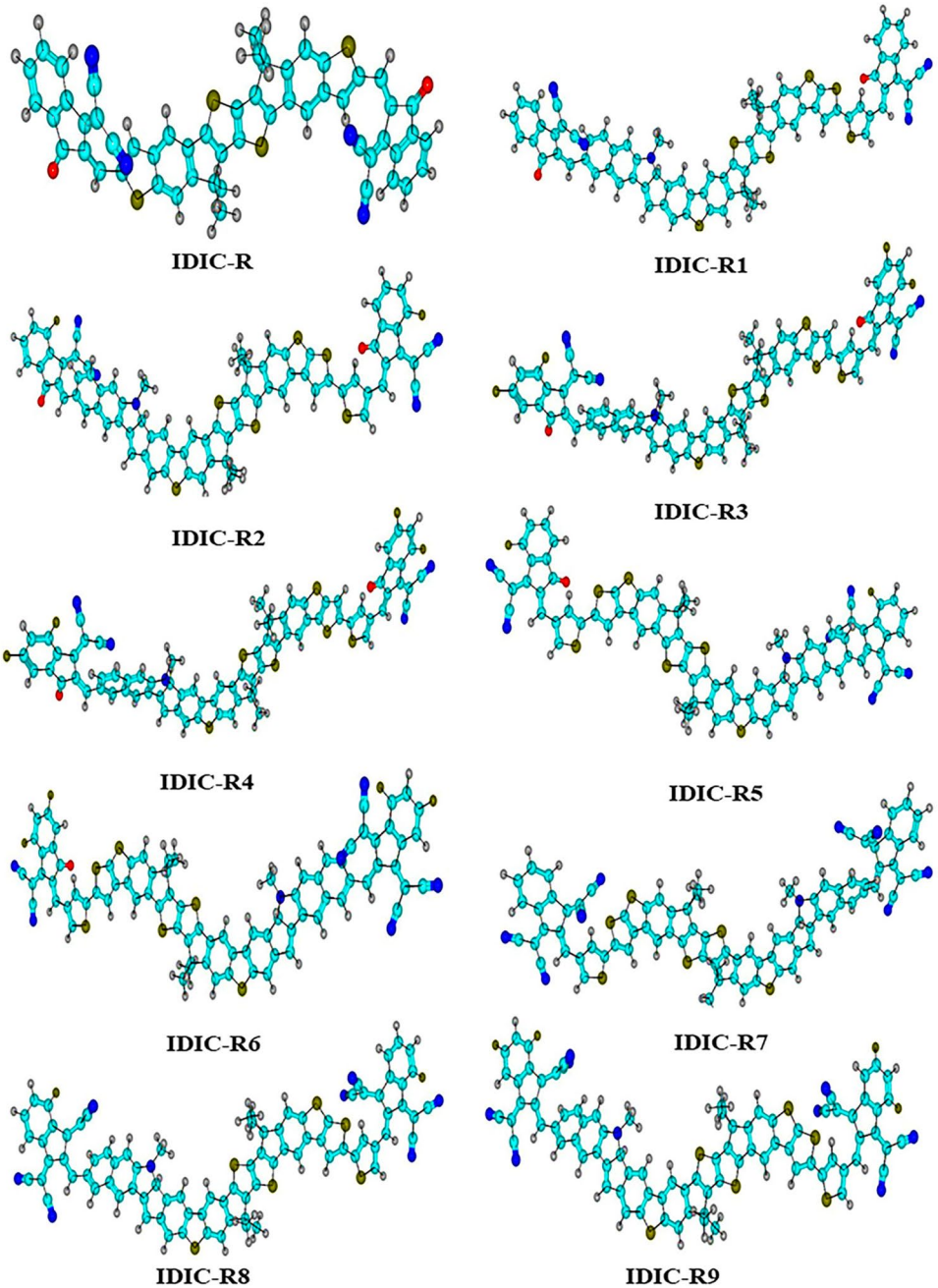

Fig. 2 Optimized geometrical structures of newly designed dyes (**IDIC-R1**–**IDIC-R9**)

DFT-based global reactivity descriptors. In addition, these descriptors can be used to create structure–activity interactions. The property to donate electrons is known as IP, while the ability to receive electrons is known as EA. Single molecular dyes with higher are expected to be more thermodynamically stable [35]. So, the overall order of IP for all the dyes were reported as **IDIC-R** (7.29) > **IDIC-R1** (7.21) = **IDIC-R2** (7.21) = **IDIC-R4** (7.21) > **IDIC-R5** (7.21) > **IDIC-R9** (7.18) > **IDIC-R7** (6.64) > **IDIC-R8** (5.91) > **IDIC** (3.32) > **IDIC-R6** (2.98) > **IDIC-R3** (2.67).

From this trend, their EA values were reported in their inverse order as in descending order: **IDIC-R5** (6.56) > **IDIC-R9** (6.53) > **IDIC-R** (6.18) > **IDIC-R4** (6.18) > **IDIC-R2** (6.02) > **IDIC-R1** (5.94) > **IDIC-R8** (5.81) > **IDIC-R7** (0.76) > **IDIC-R6** (0.76) > **IDIC-R3** (0.25) > **IDIC** (0.20). In addition, these factors are connected to orbital bandgap readings and are inversely related to the overall σ with following descending order as **IDIC-R8** (10) > **IDIC-R5** (1.54) > **IDIC-R9** (1.54) > **IDIC-R4** (0.97) > **IDIC-R** (0.9) > **IDIC-R2** (0.84) > **IDIC-R1** (0.79) > **IDIC-R6** (0.45) > **IDIC-R3** (0.41) > **IDIC** (0.32) > **IDIC-R7** (0.17). The overall order of χ was documented as follows: **IDIC-R5** (6.885) > **IDIC-R9** (6.855) > **IDIC-R** (6.73) > **IDIC-R4** (6.695) > **IDIC-R2** (6.615) > **IDIC-R1** (6.575) > **IDIC-R8** (5.86) > **IDIC-R7** (3.7) > **IDIC-R6** (1.87) > **IDIC** (1.76) > **IDIC-R3** (1.46). According to mechanics, μ is the energy that can be obtained or created because of a change in the chemical density of the defined species, or even in a chemical reaction or phase transition. Their overall order was noted as **IDIC-R3** (− 1.46) > **IDIC** (− 1.76) > **IDIC-R6** (− 1.87) > **IDIC-R7** (− 3.7) > **IDIC-R8** (− 5.86) > **IDIC-R1** (− 6.575) > **IDIC-R2** (− 6.615) > **IDIC-R4** (− 6.695) > **IDIC-R** (− 6.735) > **IDIC-R9** (− 6.855) > **IDIC-R5** (− 6.885). The dye **IDIC-R2** had the greatest IP value of 7.6 eV, indicating that the D moiety communicated the electrical potential density to the A effectively, whereas **IDIC-R6** had the smallest IP value, 6.13 eV. According to thermodynamics, the chemical potential of any entity has been the energy that may be absorbed/released due to a change in density of the specific species, or in a chemical processes or phase transitions [36]. The dye **IDIC-R3** had the highest value, which was reduced to 0.11 eV in **IDIC-R6**. The overall order was noted as **IDIC-R3** > **IDIC** > **IDIC-R6** > **IDIC-R7** > **IDIC-R5** > **IDIC-R1** > **IDIC-R2** > **IDIC-R4** > **IDIC-R** > **IDIC-R9** > **IDIC-R8**. Electrophilicity index was noted as **IDIC-R5** > **IDIC-R8** > **IDIC-R9** > **IDIC-R4** > **IDIC-R** > **IDIC-R2** > **IDIC-R1** > **IDIC** > **IDIC-R7** > **IDIC-R6** > **IDIC-R3**. The minimal bandgap revealed that the subsequent ICT interaction took place within the investigated molecule and demonstrated significant kinetics. The GRPs revealed that all the dyes were softer, with an electrophilic entity, and have a high affinity for other solar materials. According to the molecular electrostatic potential framework, the negative and positive locations of the examined chemical are located surrounding electronegative elements and hydrogen atoms.

DOS spectra

Several types of electronic states (per unit volume per unit energy) are inhabited by electrons at a quantized energy level at the Fermi level enabling DOS with an extremely high value to suggest that various sorts of states for energy condition are accessible. A zero score along the axis represents the lack of a state for excited electrons. The DOS

Table 1 Energies in eV for frontier molecular orbital (HOMO and LUMOO) with their band gaps for standard (IDIC), reference (IDIC-R), and newly designed (**IDIC-R1**–**IDIC-R9**) dyes

Dye	E_{HOMO}	E_{LUMO}	Bandgap
IDIC	− 3.32	− 0.20	3.12
IDIC-R	− 7.29	− 6.18	1.11
IDIC-R1	− 7.21	− 5.94	1.27
IDIC-R2	− 7.21	− 6.02	1.19
IDIC-R3	− 2.67	− 0.25	2.42
IDIC-R4	− 7.21	− 6.18	1.03
IDIC-R5	− 7.21	− 6.56	0.65
IDIC-R6	− 2.98	− 0.76	2.22
IDIC-R7	− 6.64	− 0.76	5.88
IDIC-R8	− 5.91	− 5.81	0.10
IDIC-R9	− 7.18	− 6.53	0.65

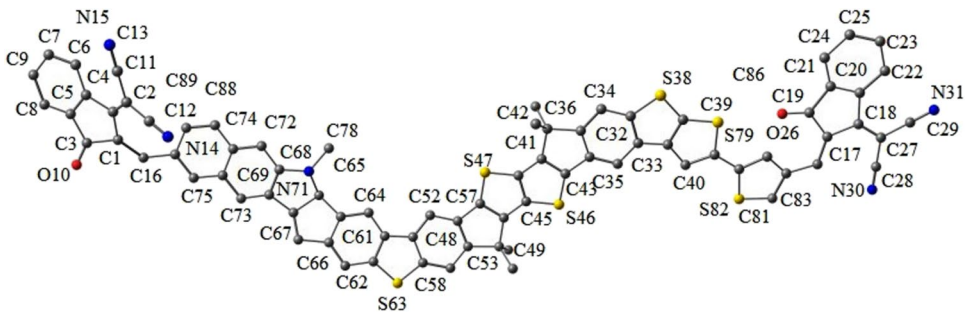

Fig. 3 Optimized geometrical structure of dyes **IDIC-R1** as a model

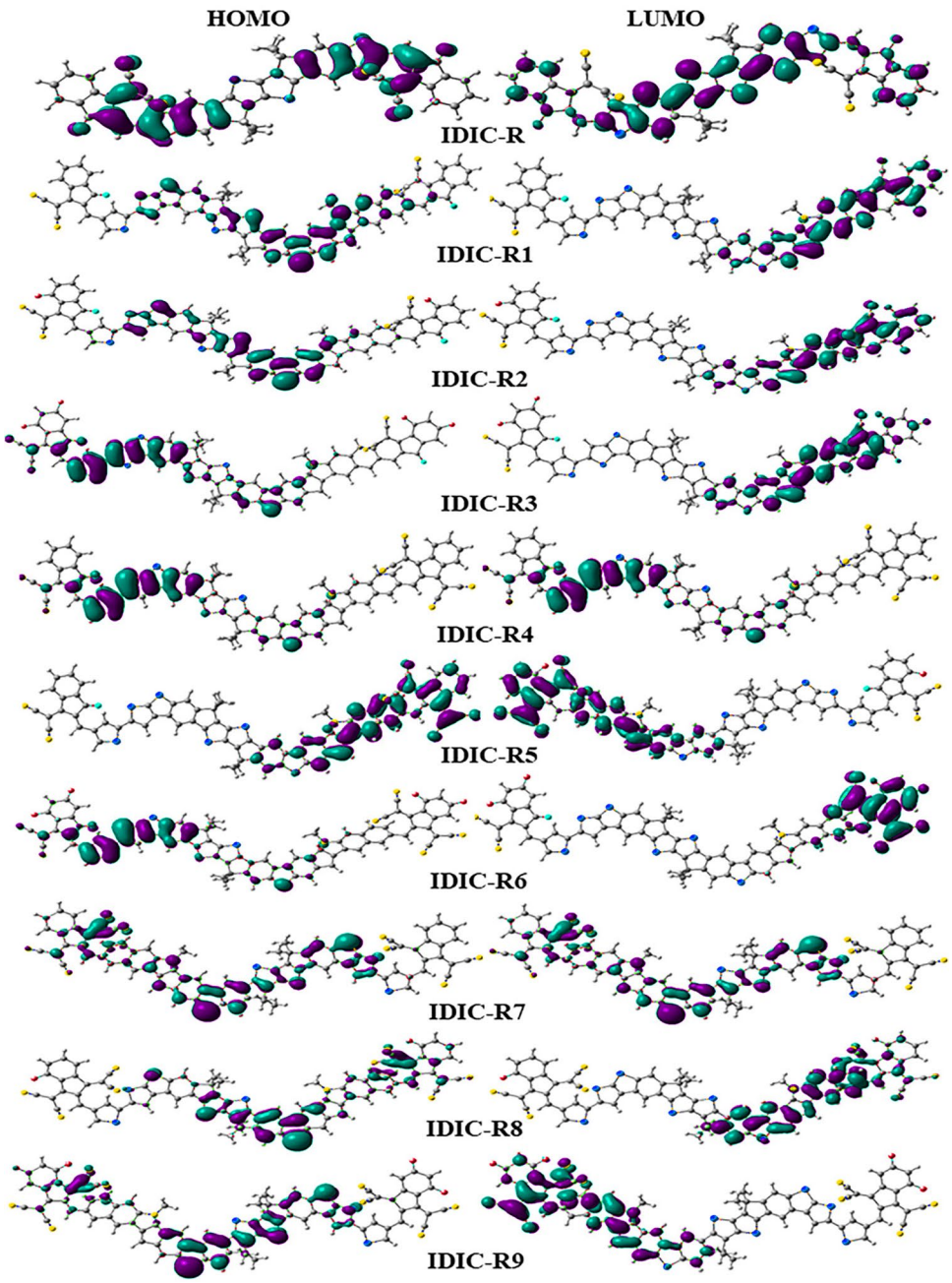

Fig. 4 FMO analysis of dyes (**IDIC-R1–IDIC-R9**) at B3LYP level

models may be used to compute the general dispersion of excited states due to energy and bandgap. The DOS graphs of the newly developed dyes were at the DFT level of theory. The A units group involvement in HOMO was 47%, whereas LUMO was 23%. All D units contributed 54–71% to HOMOs and 18–26% to LUMOs, whereas π-spacers contributed 45–49% to HOMOs and 30–43% to LUMOs (Fig. 5). These insights show that designing varied dyes by altering different effective A moiety has a significant impact on ionic and electronic cloud transparency in a variety of ways. Each dye is made up of three components: a D, a π-spacer, and an A unit. The maximal charge density of the HOMO was about 6–11 eV on that π-spacer, but the LUMO content at the D section was 1.5 eV, indicating effective ICT from D to A region via the π-spacer.

The greatest HOMO density reported in **IDIC-R2** is 7 eV, which is 45% on the π-spacer, whereas the greatest LUMO density was found only on the A, which provides 73% of the charge. For **IDIC-R3** and later, the A restricts the maximum HOMO density to 7–14 eV, while the π-spacer restricts the highest LUMO concentration to 2.4 eV, enhancing the electron-withdrawing behavior while concurrently prolonging the conjugation. All the DOS examined data strongly supports the FMO conclusions. Another key factor

Table 2 GRP analysis of dyes **IDIC-R1–IDIC-R9**

Dyes	IP	EN	χ	μ	η	σ	ω
IDIC	3.32	0.2	1.76	− 1.76	1.56	0.32	2.42
IDIC-R	7.29	6.18	6.73	− 6.735	0.555	0.90	12.59
IDIC-R1	7.21	5.94	6.575	− 6.575	0.635	0.79	13.73
IDIC-R2	7.21	6.02	6.615	− 6.615	0.595	0.84	13.02
IDIC-R3	2.67	0.25	1.46	− 1.46	1.21	0.41	1.29
IDIC-R4	7.21	6.18	6.695	− 6.695	0.515	0.97	11.54
IDIC-R5	7.21	6.56	6.885	− 6.885	0.325	1.54	7.70
IDIC-R6	2.98	0.76	1.87	− 1.87	1.11	0.45	1.94
IDIC-R7	6.64	0.76	3.7	− 3.7	2.94	0.17	20.12
IDIC-R8	5.91	5.81	5.86	− 5.86	0.05	10.00	0.86
IDIC-R9	7.18	6.53	6.855	− 6.855	0.325	1.54	7.64

that influences the optical efficiency of chromophore is light harvesting.

UV–Visible analysis

The UV–Vis analysis gives additional evidences for a wide range of electronic events [31] for DSSCs regarding their parameters of incident light absorption at specific wavelength (Fig. 6). In addition, some other relevant features by which several DSSC-related parameters such as their λ_{max}, transition energy (E), and oscillator strength (f^{os}) can be calculated. Those values were calculated in gaseous phase using TD-DFT simulations to pictograph typical absorption changes in the dyes **IDIC-R1–IDIC-R9** with an inverse relationship between their E and λ_{max}. Photovoltaic cells are wavelength selective and respond positively to sunlight in some areas of the spectrum than others, generally a wavelength range of 600–700 nm. Generally, the greater the frequency of light with more energy carried by emitted electrons, the smaller the wavelength of incident beam. Similarly, the absorption λ_{max}, f^{os}, and E for the identical spectral allocations in increasing solvent polarity from methanol through dichloromethane to chloroform were calculated and had a λ_{max} of 476–483 nm with redshift. The average λ_{max} values (nm) were recorded in the following order: **IDIC-R2** (881) > **IDIC-R8** (498) > **IDIC-R5** (492) > **IDIC-R9** (489) > **IDIC-R7** (487) > **IDIC-R1** (486) > **IDIC-R6** (486) > **IDIC-R** (479) > **IDIC** (476) > **IDIC-R4** (378) > **IDIC-R3** (375). The dye **IDIC** has the smallest λ_{max} value among the dyes produced. The experimentally acquired absorption spectra of the reference molecule match the estimated results (Table 3). The analysis revealed that electron-withdrawing end-capped A units had such a significant influence on peak value. This electron-deficient constituent is responsible for the red shift in absorption spectra. All the dyes **IDIC-R1–IDIC-R9** had absorption band widths extending from 480 to 498 mm, which are red shifted in contrast to **IDIC**. The dyes **IDIC-R2** and **IDIC-R6** demonstrated a stronger red shift with lowest E values of 1.28 and 0.77 eV, respectively.

Because of the low bandgap, charge separation might be possible there [37]. The dyes **IDIC-R1**, **IDIC-R3**, and **IDIC-R4** exhibited identical λ_{max} values, with their values of f^{os} at 0.0034–0.39. All the dyes (**IDIC-R1–IDIC-R9)** showed E ranging from 0.77 to 1.66 eV, which had been lower than the typical value of 1.743 eV. The computed fluorescence emission of such relevant dye structures in chloroform was well given the previously published data. It also implies that the H-bond to the lone pairs of alkene units in S^1 states was disrupted in the solvent trap by the transport of lone pairs to certain ring following excitation.

As a result, the CT functionality is included in the allowed transition. Because of the above discussion, it is possible to conclude that the newly designed dyes have superior optoelectronic characteristics than the reference dye molecule. All the dyes that have recently been created are thought to have high values of E, f^{os}, and absorption coefficients. The dye **IDIC-R3** and **IDIC-R6** could be used as key fullerene free D subunits in PV systems.

Optical performance is influenced by a segment called light harvesting efficiency (LHE). The greatest charge transfer (CT) sensitivity is found in dyes with a high LHE content. The formula can be used to calculate the LHE of dyes. In spectroscopic calculations, oscillator strength is a non-dimensional variable that reflects the likelihood of incident electromagnetic absorption/emissions during transitions as energy. Non-radioactive decay can beat optical decay if particle emitters with state do have low oscillator intensity. The greater the CT inside the semiconductor, the greater is the LHE. It was calculated using the oscillator intensity of the UV–Vis analysis. The following is the general order of all the values, in decreasing order: **IDIC-R1** (0.0796) > **IDIC-R8** (0.0753) > **IDIC-R7** (0.067) > **IDIC-R3** (0.0379) > **IDIC-R5** (0.0252) > **IDIC-R4** (0.0241) > **IDIC-R6** (0.023) > **IDIC-R2**

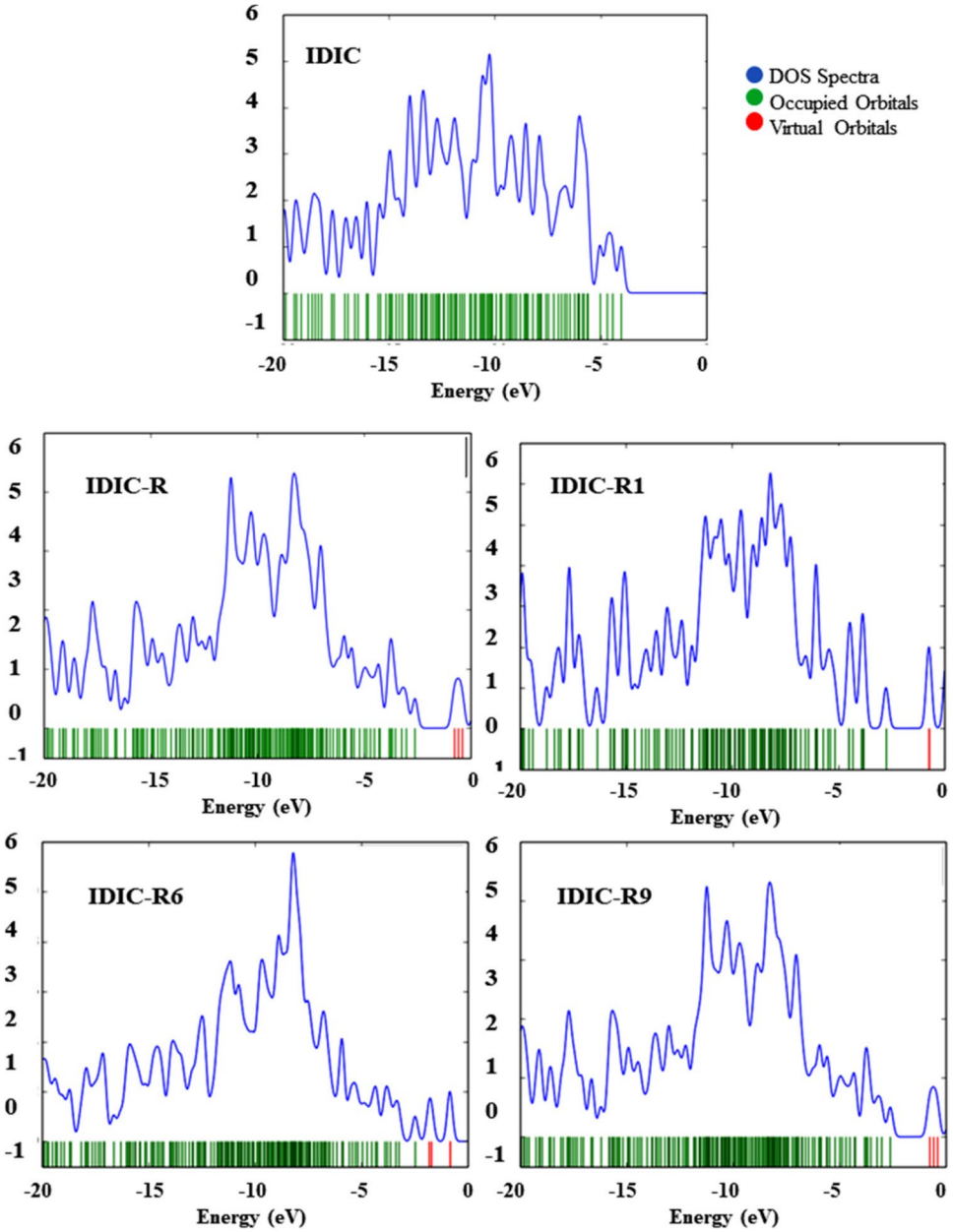

Fig. 5 A comparative analysis of **DOS** spectra of newly designed dyes with **IDIC** and **IDIC-1**

(0.0092) > **IDIC** (0.0078) > **IDIC-R** (0.0078) > **IDIC-R9** (0.0053).

NBO analysis

NBO research assists in the finding of hydrogen bonds in engineered molecules that result from hyper conjugated engagements [38]. It provides a realistic image for investigating intra-molecular delocalization and electron density as the units get beyond electron D to A units. As the energy of stabilization grows, the interaction across the D unit functionalities becomes more essential. Equation (12) is the stabilizing energy formula employing a second-order perturbation approach.

$$E^{(2)} = q_i \frac{\left(F_{i,j}\right)^2}{\varepsilon_j - \varepsilon_i} \tag{12}$$

q_i represents D units orbital availability, whereas $E^{(2)}$ denotes stabilization energy, $F_{i,j}$ symbolizes off-diagonal NBO Fock parameter, and j and i signify diagonal components. An NBO examination is a practical method for investigating conjugative cooperation or electrostatic interactions in microscopic arrangements to uncover intra-atomic and microscopic anchoring and connections between bonds. For

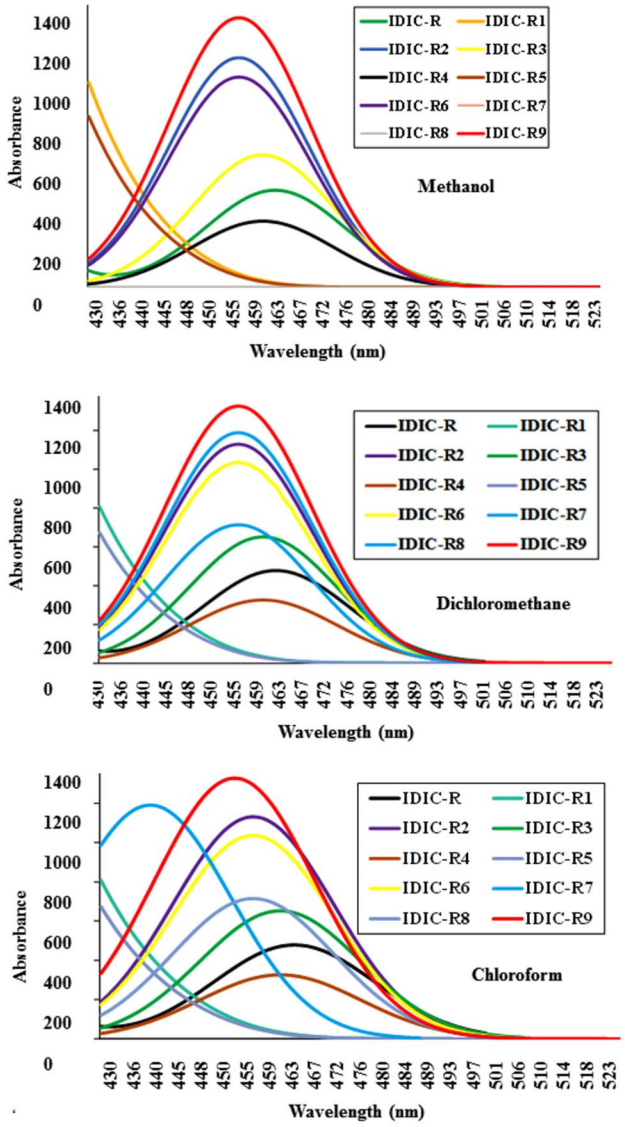

Fig. 6 Computed UV–Visible spectra of dyes (**IDIC-R1–IDIC-R9**) in chloroform

dyes **IDIC-R1** and **IDIC-R2**, an NBO analysis was conducted and enlarged, and some important data are shown in Table 4. The biggest value of a feasible transition was observed at 30.02 kcal/mol (S63)LP→(C61-C62) π^* transitions, which was also identified as the most dependable transition in generating the maximum stabilization energy and a forceful interaction of D and A components. The transition from (C2-C11)π→(C1-C2)π^*, (C1-C16)π→(C90-C91) π^*, was rated with the least stabilization energies having a stabilization energy of 0.65 kcal/mol. For dye **IDIC-R**, the most prominent transitions were noted as (C1-C2) π→C1-C16π* which had the stabilization energy range of 0.75, 1.18, and 0.027 kcal/mol for D units, π-linker, and A units, respectively.

In dye **IDIC-R1**, the transition (C1-C2)π→(C2-C4) π* had the stabilization energy ranges of 0.76, 1.01, and 0.025 kcal/mol for D, π, and A units, respectively. In dye **IDIC-R2**, the transition (O26)LP→(C19-O26)π^* had the stabilization energy ranges of 0.74, 0.63, and 0.020 kcal/mol for D, π-spacer, and A units, respectively. The outputs of these stabilization energies are created by a weak interaction between being D and A. The best significant transition for π* revealed by **IDIC-R3** was (C2-C4)π→(C3-C5)π* which had the stabilization energy of 1.27, 1.04, and 0.033 kcal/mol for D, π-spacers, and A units, respectively. For **IDIC-R4**, the significant transitions of (C3-O10)π→(C3-C5)π* were noted with 0.69, 1.31, and 0.028 stabilization energies for D, π-spacers, and A units, respectively. For **IDIC-R5**, the noticeable transitions were acquired as (S82)LP→(C84-C85)π* with the stabilization energies of 0.64, 1.13, and 0.024 kcal/mol for D, π-spacers, and A units, respectively. Due to resonance [39], further electronic transitions displayed stabilization energies with the lowest stabilization energy value of 0.13 kcal/mol in **IDIC-R6** for transitions such as (S38)LP→(C39-C40)π* with stabilization energies of 0.67, 1.17, and 0.025 kcal/mol for D, π-spacers, and A units, respectively. The good quality significant transition revealed by **IDIC-R7** was (C1-C2)π→(C1-C11)π* which

Table 3 Absorption and other photovoltaic related parameters of dyes **IDIC-R1–IDIC-R9**

Dyes	*E*	λ_{max}	f^0	LHE	μ_{gm}	Major transitions (%)
IDIC	2.12	476	0.0034	0.0078	3.02	H→L (89)
IDIC-R	1.32	479	0.0034	0.0078	2.32	H-1→L (82)
IDIC-R1	1.66	486	0.036	0.0796	3.02	H→L (71)
IDIC-R2	1.28	881	0.0040	0.0092	2.32	H-1→L (79)
IDIC-R3	1.59	489	0.0168	0.0379	1.27	H-1→L (52)
IDIC-R4	0.39	498	0.0106	0.0241	3.51	H→L (71)
IDIC-R5	0.76	492	0.0111	0.0252	2.75	H→L+1 (44)
IDIC-R6	0.77	486	0.0101	0.0230	3.01	H→L (73)
IDIC-R7	0.45	487	0.0301	0.0670	3.16	H-1→L (79)
IDIC-R8	1.21	498	0.034	0.0753	2.19	H-1→L (50)
IDIC-R9	0.98	489	0.0023	0.0053	3.21	H→L (70)

had the stabilization energy of 0.51, 1.18, and 0.022 for D, π, and A units, respectively. The good quality significant transition revealed by **IDIC-R8** was (C1-C3)π → (C4-C5) π* which had the stabilization energy of 0.94, 1.18, and 0.030 for D, π-spacers, and A units, respectively. The best significant transition for * revealed by **IDIC-R9** was (C1-C3)π → (C16-C91)π* which had the stabilization energy of 2.56, 1.06, and 0.047 kcal/mol for D, π-spacers, and A units, respectively, whereas transfer (S46)LP → (C42-C43)π*, (C1-C3)π → (C16-C91)π* had the lowest stabilization energy of 0.65 kcal/mol. The results also showed that the delocalized antibonding orbital angular momentum, together with their corresponding bonding orbitals, plays a crucial role in band stability and significant structural design. It is reasonable to assume that the extended conjugation observed in **IDIC-R1–IDIC-R9** was necessary for stabilization.

Open-circuit voltage

As stated by Schwarber and colleagues about $HOMO_D \rightarrow LUMO_A$ energy fluctuations, dyes were used for their open circuit by evaluating D unit moieties for its strength. The V_{oc} ranged from − 1.82 to 0.72 eV for newly discovered dyes. For a benchmarking reference, **IDIC** was employed as a standard D component. Except for **IDIC-R6**, all the readings are negative. The dyes **IDIC-R1–IDIC-R5** had negative voltage, indicating an OFF state, while **IDIC-R1–IDIC-R3, IDIC-R5, IDIC-R6, IDIC-R8**, and **IDIC-R9** had a positive value, indicating an ON condition (Fig. 7). Using **IDIC** as a reference, the negative values were revealed because when **IDIC-R6** was turned on, the passage of open-circuit voltage would function in an OFF condition.

Electron injection and hole analysis

As work function (W) of metal (HIE = E_{HOMO}) and (EIE = E_{LUMO}), a hole/electron injection barrier (HIE/EIE) [40] originating from dyes and toward the aluminum (Al) and gold (Au) electrodes is being investigated. In the HIE of new dyes for Au metal, the decreasing rank was as follows: **IDIC-R1** (− 0.77) > **IDIC-R3** (− 0.93) > **IDIC-R4** (− 1.54) > **IDIC-R6** (− 1.71) > **IDIC-R5** (− 1.8) > **IDIC-R2** (− 1.88) (Table 5). It was emphasized for Al in the following order: **IDIC-R2** (3.18) > **IDIC-R5** (3.16) > **IDIC-R3** (3.14) > **IDIC-R4** (2.99) > **IDIC-R1** (2.37) > **IDIC-R6** (1.71). The introduction of the dyes with Au and Al electrodes produced some surprising findings for EIE as follows: **IDIC-R1** (− 0.49) > **IDIC-R3** (− 0.65) > **IDIC-R4** (− 1.26) > **IDIC-R6** (− 1.43) > **IDIC-R5** (− 1.52) > **IDIC-R2** (− 1.52) (− 1.6) **IDIC-R2** (11.8) > **IDIC-R5** (11.78) > **IDIC-R3** (11.76) > **IDIC-R4** (11.61) > **IDIC-R1** (10.99) > **IDIC-R6** (10.33). Depending on electron injection and hole analysis, all dyes can operate as good electrochemical devices, and the electrode impact is non-existent. They also represent the same metal trend. However, it can be deduced that Au

Table 4 NBO analysis newly derived dyes (**IDIC-R1–IDIC-R9**)

Dye	D (*i*)	Type	A (*j*)	Type	$E^{(2)}$	$E(j)E(i)$ kcal/mol	$F_{i,j}$ kcal/mol
IDIC-R	C1-C2	π	C1-C16	π*	0.75	1.18	0.027
	O10	LP	C3-C5	π*	27.12	0.63	0.119
IDIC-R1	C1-C2	π	C2-C4	π*	0.76	1.01	0.025
	N14	LP	C11-C12	π*	5.72	0.99	0.068
IDIC-R2	C1-C2	π	C2-C11	π*	0.90	1.14	0.029
	O26	LP	C19-O26	π*	0.74	0.63	0.020
IDIC-R3	C2-C4	π	C3-C5	π*	1.27	1.04	0.033
	S63	LP	C61-C62	π*	30.20	0.26	0.082
IDIC-R4	C3-O10	π	C3-C5	π*	0.69	1.31	0.028
	S79	LP	C80-C81	π*	0.70	1.14	0.025
IDIC-R5	C1-C2	π	C4-C5	π*	0.98	1.16	0.030
	S82	LP	C84-C85	π*	0.64	1.13	0.024
IDIC-R6	C1-C2	π	C11-C12	π*	1.05	1.04	0.029
	S38	LP	C39-C40	π*	0.67	1.17	0.025
IDIC-R7	C1-C2	π	C1-C11	π*	0.51	1.18	0.022
	S46	π	C44-C45	π*	0.73	1.15	0.026
IDIC-R8	C1-C3	π	C4-C5	π*	0.94	1.18	0.030
	S46	π	C42-C43	π*	32.34	0.28	0.086
IDIC-R9	C1-C3	π	C16-C91	π*	2.56	1.06	0.047
	S46	π	C44-C45	π*	32.39	0.25	0.085

is a good choice for electron hole research, but Al is an outstanding electrode choice for electron injection study.

Charge tripping analysis

To investigate the possible use of D functions in OSC semiconductors, the **IDIC-R8** was coupled with **IDIC** as a complex and optimized at B3LYP functionality at its energy minima. The complex of both dyes was optimized to its ground state energy by using PBEEPBE basis set at DFT level [41]. We decided to note the pathway of electron transfer for the **IDIC-R8** as it had the highest V_{oc}. Also, the dye **IDIC** had been a well synthetic solar dye that was also frequently used in CT. We applied our produced dyes on the D component to measure the efficiency of ICT. In HOMO, a developed electrical environment is focused over **IDIC-R8**, but in LUMO, it is concentrated over the **IDIC/IDIC-R8** complex, including its final stage A part (Fig. 8).

Because of the efficient flow of electrons from D to A, these dyes are appropriate OSCs to be used in organic semiconductor technologies. Furthermore, its bandgap was found at 1.11 eV which was manageable for plausible electronic transitions. The method was used to forecast transition behavior, particularly from a shorter wavelength to the singlet excited state (S_1), as well as D-A unit interactions with charge carrier localization. Hydrogen atoms were left out since their effect on such changes is so minor.

NLO response

Non-linear optical (NLO) response is effective in organic molecules with sufficient electrical connection across their various moieties (Fig. 9) [4]. Many computational and experimental investigators have focused on materials engineering, thermodynamics, and their chemistry to quest for new and efficient NLO responsive materials [42]. Interdisciplinary efforts to create NLO materials have been initiated

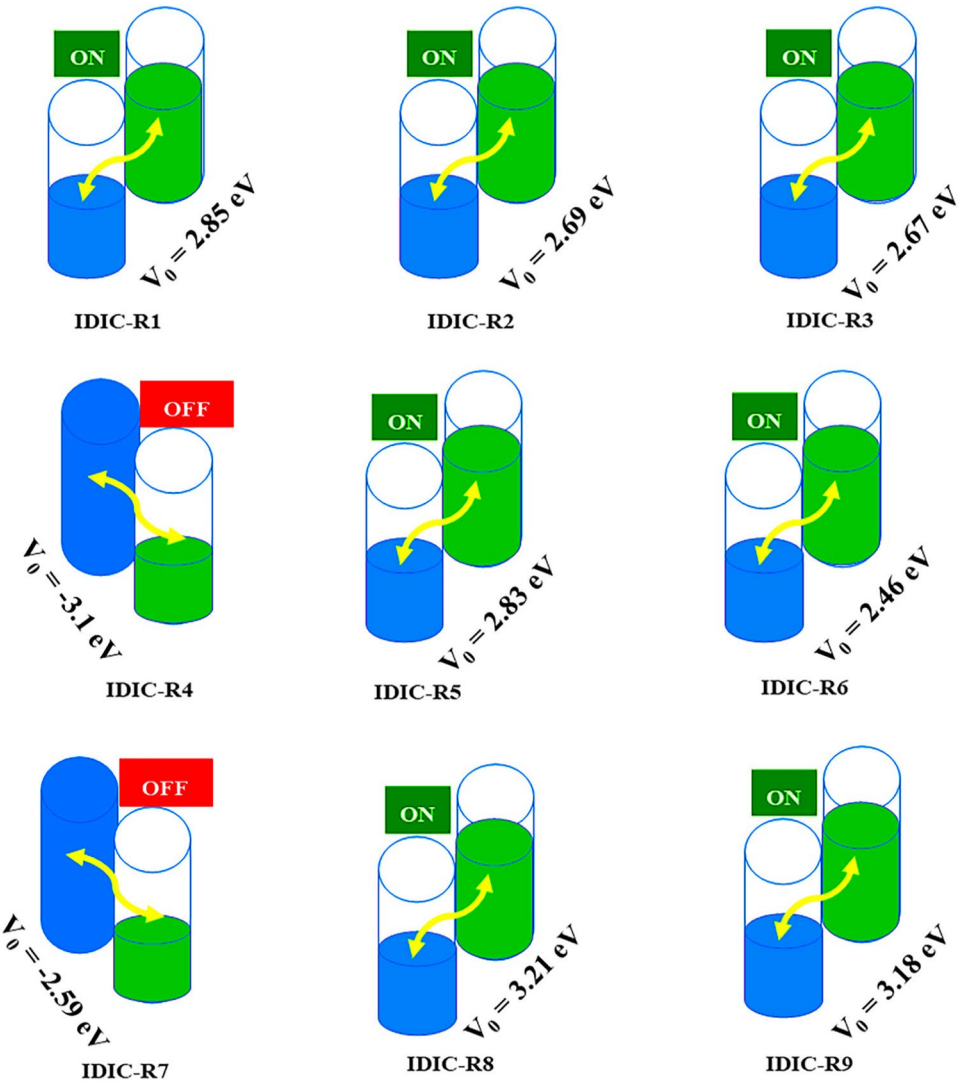

Fig. 7 The V_{oc} of newly designed dyes (**IDIC-R1**–**IDIC-R9**) with **IDIC-R** in chloroform

Table 5 **HIE/EIE** analysis of newly designed dyes (**IDIC-R1–IDIC-R9**)

Dye	HIE (Au)	EIE (Au)	HIE (Al)	EIE (Al)
IDIC-R	2.87	− 1.70	11.49	− 1.98
IDIC-R1	2.79	− 1.46	11.41	− 1.74
IDIC-R2	2.79	− 1.54	11.41	− 1.82
IDIC-R3	− 1.75	4.23	6.87	3.95
IDIC-R4	2.79	− 1.70	11.41	− 1.98
IDIC-R5	1.49	− 1.33	10.11	− 1.61
IDIC-R6	− 1.44	3.72	7.18	3.44
IDIC-R7	2.22	3.72	10.84	3.44
IDIC-R8	2.79	− 2.08	11.41	− 2.36
IDIC-R9	2.76	− 2.05	11.38	− 2.33

as the need for photonic manipulation, harmonic production, frequency melding, and accompanying statistics rises [43]. During the present study, the electronic features were used to estimate the amplitude of optical engagements to monitor a sequential linear relationship (polarizability) and non-linear responses (hyperpolarizabilities) [44]. The calculated α_{total} and β_{total} values of the dyes were recommended. All tensors stated were employed as a reference material for a measurement of initial hyperpolarizability and magnetic moments, and they were determined to be greater than those for the literature. All dyes were discovered to have more μ_{nor} than urea (1.373 D) with the following order in descending values: **IDIC-R4** (3.51) > **IDIC-R9** (3.21) > **IDIC-R7** (3.16) > **IDIC-R1** (3.02) > **IDIC** (3.02) > **IDIC-R6** (3.01) > **IDIC-R5** (2.75) > **IDIC-R2** (2.32) > **IDIC-R** (2.32) > **IDIC-R8** (2.19) > **IDIC-R3** (1.27). The dye **IDIC-R5** has the highest μ_{nor} (8.72 D) of any molecule synthesized. The overall descending sequence of hyperpolarizability (D) values was **IDIC-R9** (1055) > **IDIC-R8** (994) > **IDIC-R7** (934) > **IDIC-R6** (874) > **IDIC-R5** (667) > **IDIC-R4** (580) > **IDIC-R** (521) > **IDIC-R2** (470) > **IDIC-R1** (439) > **IDIC-R3** (354). The larger the μ_{nor} value, the lower the bandgap, resulting in an excellent NLO value observed. The recommended compound IDIC-**R5** was proven to have the greatest mean polarizability. In addition, 3485 D, a noteworthy rise in its value, was identified. The inclusion of three nitro groups boosted electron-withdrawing ability by enriching the electrical structure surrounding the A unit.

The intensity of substituents applied to the A unit (**PD6**) influenced a molecule with its non-linearity. When replacements occur, conjugated contribution grows and becomes more dominant. The overall worth was arranged in decreasing order. The dye **IDIC-R5** is more functional than **IDIC-R6**. The dye **IDIC-R5** offers the highest overall value when compared to other created dyes.

A comparison study was carried out using urea as a reference component, yielding a β_{tot} value of 714 D. The dye **IDIC-R1** and **IDIC-R6** showed hyperpolarizability values that were 8.33 and 1.27 times greater, respectively, than the standard. The NLO responses exhibited in **IDIC-R1** to **IDIC-R9** are bigger because of stronger electron-withdrawing entities in the acceptor half, which may minimize the HOMO → LUMO band gap, boost the ICT between both

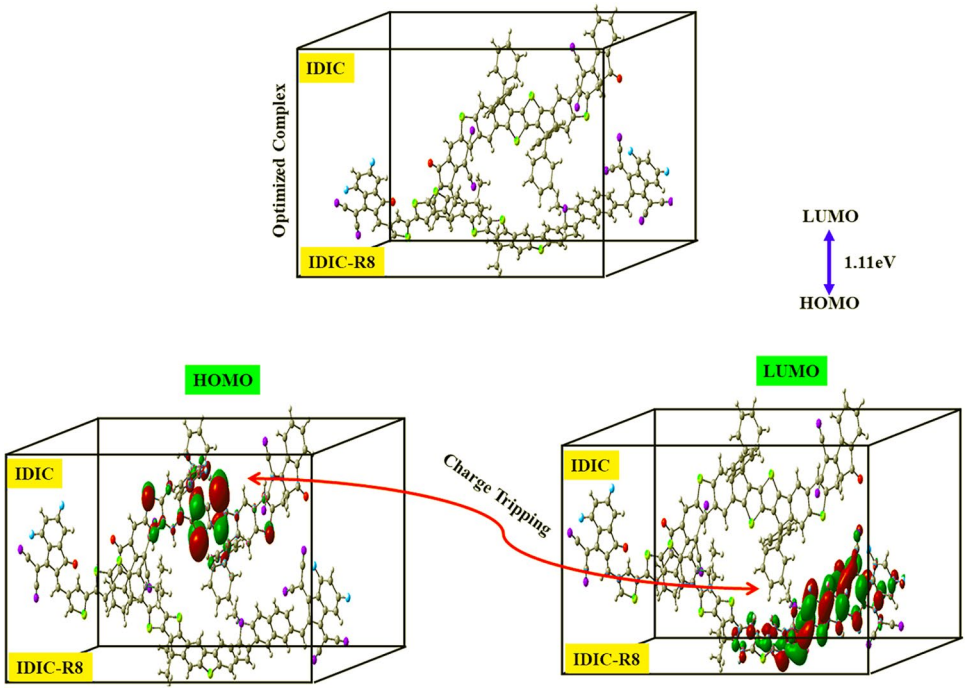

Fig. 8 Charge tripping analysis of optimized complex between dye **IDIC-R8** and **IDIC** at DFT

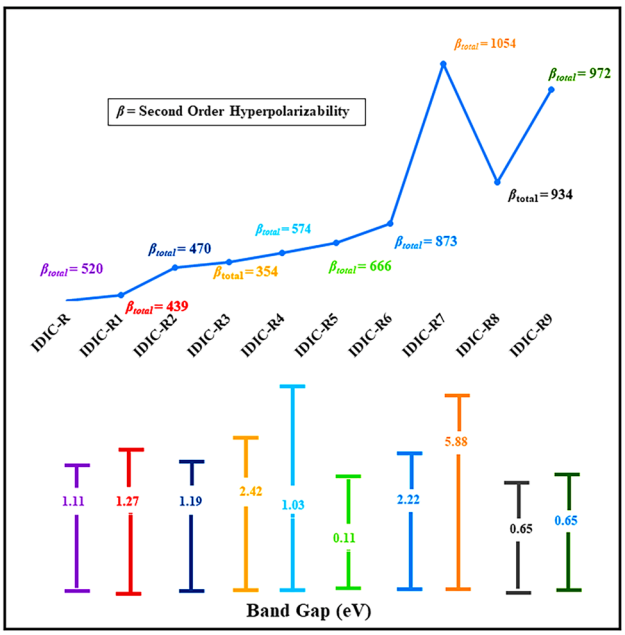

Fig. 9 Graphical representation of NLO response as a function of their band gaps for newly designed dyes (**IDIC-R1–IDIC-R9**)

orbitals, and then further polarize the molecule. When the bandgap between the HOMO and LUMO orbitals were inverted, all the recommended dyes exhibited second-order hyperpolarizability numbers. The dye **IDIC-R8** is the most valuable. The current work dives into the fascinating NLO recordings of conjugated push–pull organic compounds for modern optical applications. Furthermore, because of their significant NLO sensitivity, the created dyes can be used as study targets.

Conclusions

Organic compounds that have significant non-linear optical (NLO) properties are widely employed in the optical device sector. Nine newly designed, *Pull–Push*, organic dyes (**IDIC-R1–IDIC-R9**) with A-π-D-π-D-π-A framework were theoretically generated from A and D components with π-spacers by changing the different substituted opportunities to automate their band gap and their NLO responses. The influence of various A units on non-linear kinetic energy modes is examined. FMO tests revealed that all the created dyes had a very small bandgap which had a reflection of their effect in their other PV properties. These GRP values were shown to be associated with a shorter bandgap, with lower values and higher σ scores. Furthermore, when compared to the reference molecule, all the dyes had greater λ_{max} values and slightly lower energy of electronic transitions. An NBO investigation demonstrated the creation of electrostatic repulsion in molecules between the D and A species. Such charge separation might be the result of a significant NLO reaction due to ICT from D to A. The initial hyperpolarizability indices of the dyes **IDIC-R1–IDIC-R9** were eight times higher than those of the reference molecule. The most valuable dye is **IDIC-R8**. Our findings should help in the development of organic dyes with desirable characteristics for improving optical device efficiency. Also, a pull–push effect can be generated to enhance the NLO responses by using π-poor versus π-rich electronic dyes toward the dye-sensitized solar cells. Among all the dyes, **IDIC-R8** produced the highest V_{oc} value and at the same time it also had the highest second-order NLO response to imply that this dye structure can be a good candidate to be synthesized experimentally. Due to their appealing characteristics including cheap cost, simplicity of manufacture, transparency, and high performance under normal situations, these improvements may serve as the foundation for the global acceptance of DSSCs as energy harvesters.

Supplementary Information The online version contains supplementary material available at https://doi.org/10.1007/s00894-022-05402-6.

Acknowledgements The authors thank the University of Gujrat, Gujrat, Pakistan, for providing access to all research facilities.

Author contribution Conceptualization: SHS. Methodology: AUH. Formal analysis and investigation: MFN. Writing—original draft preparation: AUH. Writing—review and editing: GM. Resources: MNZ.

Data availability All data generated or analyzed during this study are included in this published article and its supplementary information file.

Code availability Gaussian 09 W and GaussView 5.1 are used for simulation, and Origin software is used to draw the plots.

Declarations

Consent to participate This article does not contain any studies with human participants or animals, clinical trial registration, or plant reproducibility performed by any author.

Consent for publication All authors have approved the paper and agree to its publication.

Human and Animal Rights This work did not involve any human subjects.

Conflict of interest The authors declare no competing interests.

References

1. Fernandes RV, Urbano A, Duarte JL et al (2018) Tuning the optical properties of luminescent down shifting layers based on organic dyes to increase the efficiency and lifetime of P3HT: PCBM photovoltaic devices. J Lumin 203:165–171. https://doi.org/10.1016/j.jlumin.2018.06.053

2. Qian G, Wang ZY (2010) Near-infrared organic compounds and emerging applications. Chem Asian J 5:1006–1029. https://doi.org/10.1002/asia.200900596
3. Badawy WA (2015) A review on solar cells from Si-single crystals to porous materials and quantum dots. J Adv Res 6:123–132. https://doi.org/10.1016/j.jare.2013.10.001
4. Hassan AU, Mohyuddin A, Güleryüz C et al (2022) Novel pull–push organic switches with D–π–A structural designs: computational design of star shape organic materials. Struct Chem. https://doi.org/10.1007/s11224-022-01983-3
5. Preat J, Michaux C, Jacquemin D, Perpe EA (2009) Enhanced efficiency of organic dye-sensitized solar cells : triphenylamine derivatives 113:16821–16833. https://doi.org/10.1021/jp904946a
6. Kan B, Kan Y, Zuo L et al (2021) Recent progress on all-small molecule organic solar cells using small-molecule nonfullerene acceptors. InfoMat 3:175–200. https://doi.org/10.1002/inf2.12163
7. Hassan AU, Sumrra SH, Zafar W et al (2022) (2022) Enriching the compositional tailoring of NLO responsive dyes with diversity oriented electron acceptors as visible light harvesters: A DFT/TD-DFT approach. Mol Phy. https://doi.org/10.1080/00268976214858 5
8. Resch-Genger U, Grabolle M, Cavaliere-Jaricot S et al (2008) Quantum dots versus organic dyes as fluorescent labels. Nat Methods 5:763–775. https://doi.org/10.1038/nmeth.1248
9. Hassan AU, Sumrra SH, Nkungli NK, Güleryüz C (2022) Theoretical probing of 3d nano metallic clusters as next generation non-linear optical materials. Results Chem 4:100627. https://doi.org/10.1016/j.rechem.2022.100627
10. Holcombe TW, Norton JE, Rivnay J et al (2011) Steric control of the donor/acceptor interface: implications in organic photovoltaic charge generation. J Am Chem Soc 133:12106–12114. https://doi.org/10.1021/ja203235z
11. Innocenzi P, Lebeau B (2005) Organic-inorganic hybrid materials for non-linear optics. J Mater Chem 15:3821–3831. https://doi.org/10.1039/B506028A
12. Pramod AG, Nadaf YF, Renuka CG (2019) A combined experimental theoretical approach for energy gap determination, photophysical, photostable, optoelectronic, NLO, and organic light emitting diode (OLED) application: synthesized coumarin derivative. J Mol Struct 1194:271–283. https://doi.org/10.1016/j.molstruc.2019.05.099
13. Zhang S, Ocheje MU, Huang L et al (2019) The critical role of electron-donating thiophene groups on the mechanical and thermal properties of donor–acceptor semiconducting polymers. Adv Electron Mater 5:1800899. https://doi.org/10.1002/aelm.201800899
14. Ali U, Javed A, Tallat A et al (2019) Molecular designing of four high performance pyrazine-based non-fullerene acceptor materials with naphthalene diimide-based small organic solar cells. J Mol Model 25:50. https://doi.org/10.1007/s00894-019-3932-8
15. Etabti H, Fitri A, Benjelloun AT et al (2021) Benzocarbazole-based D-Di–π–A dyes for DSSCs: DFT/TD-DFT study of influence of auxiliary donors on the performance of free dye and dye–TiO2 interface. Res Chem Intermed 47:4257–4280. https://doi.org/10.1007/s11164-021-04531-6
16. Shanmuga Sundar GJ, Ravi Kumar SM, Sagayaraj P et al (2021) Structural, mechanical, thermal, electrical, second-and third-order nonlinear optical characteristics of MCBT NLO crystal for optoelectronics device and laser applications. Bull Mater Sci 44:1–8. https://doi.org/10.1007/s12034-021-02491-6
17. Hassan AU, Sumrra SH (2022) Exploration of pull–push effect for novel photovoltaic dyes with A–π–D design: a DFT/TD-DFT investigation. J Fluoresc. https://doi.org/10.1007/s10895-022-03003-3
18. Wang J, Zhan X (2020) Fused-ring electron acceptors for photovoltaics and beyond. Acc Chem Res 54:132–143. https://doi.org/10.1021/acs.accounts.0c00575
19. Boser SR, Mauad T, De Araújo-Paulino BB et al (2017) Myofibroblasts are increased in the lung parenchyma in asthma. PLoS ONE 12:1–14. https://doi.org/10.1371/journal.pone.0182378
20. Ajmal M, Ali U, Javed A et al (2019) Designing indaceno thiophene–based three new molecules containing non-fullerene acceptors as strong electron withdrawing groups with DFT approaches. J Mol Model 25:311. https://doi.org/10.1007/s00894-019-4198-x
21. Cheng P, Li G, Zhan X, Yang Y (2018) Next-generation organic photovoltaics based on non-fullerene acceptors. Nat Photonics 12:131–142. https://doi.org/10.1038/s41566-018-0104-9
22. Na S-I, Yu B-K, Kim S-S et al (2010) Fully spray-coated ITO-free organic solar cells for low-cost power generation. Sol Energy Mater Sol Cells 94:1333–1337. https://doi.org/10.1016/j.solmat.2010.01.003
23. Nebbach D, Agda F, Lakhlifi T et al (2022) Designing new donors organic compounds with IDIC core for photovoltaic application. Optik 262:169174. https://doi.org/10.1016/j.ijleo.2022.169174
24. Frisch MJ, Trucks GW, Schlegel HB, et al (2016) G16_C01. Gaussian 16, Revision C.01, Gaussian, Inc., Wallin
25. Sham LJ, Schlüter M (1983) Density-functional theory of the energy gap. Phys Rev Lett 51:1888
26. Hassan AU, Sumrra SH (2022) Exploring the bioactive sites of new sulfonamide metal chelates for multi-drug resistance: an experimental versus theoretical design. J Inorg Organomet Polym Mater 32:513–535. https://doi.org/10.1007/s10904-021-02135-6
27. Wei LI, Xie H, Huang Y et al (2016) Application of Gaussian 09/GaussView 5.0 in analytical chemistry teaching. J Kunming Med Univ 37:134–136
28. Hanwell MD, Curtis DE, Lonie DC et al (2012) Avogadro: an advanced semantic chemical editor, visualization, and analysis platform. J Cheminform 4:17. https://doi.org/10.1186/1758-2946-4-17
29. Zhurko GA, Zhurko DA (2009) ChemCraft, version 1.6. URL http//www chemcraftprog com
30. Sumrra SH, Hassan AU, Zafar MN et al (2022) Metal incorporated sulfonamides as promising multidrug targets: combined enzyme inhibitory, antimicrobial, antioxidant and theoretical exploration. J Mol Struct 1250:131710. https://doi.org/10.1016/j.molstruc.2021.131710
31. Hassan AU, Sumrra SH, Imran M, Chohan ZH (2022) New 3d multifunctional metal chelates of sulfonamide: spectral, vibrational, molecular modeling, DFT, medicinal and *in silico* studies. J Mol Struct 1254:132305. https://doi.org/10.1016/j.molstruc.2021.132305
32. Singh Y, Patel RN, Patel SK et al (2019) Experimental and quantum computational study of two new bridged copper(II) coordination complexes as possible models for antioxidant superoxide dismutase: Molecular structures, X-band electron paramagnetic spectra and cryogenic magnetic properties. Polyhedron 171:155–171. https://doi.org/10.1016/j.poly.2019.07.015
33. De Angelis F, Fantacci S, Selloni A et al (2010) First-principles modeling of the adsorption geometry and electronic structure of Ru(II) dyes on extended TiO_2 substrates for dye-sensitized solar cell applications. J Phys Chem C 114:6054–6061. https://doi.org/10.1021/jp911663k
34. Hassan AU, Sumrra SH, Zubair M et al (2022) Structurally modulated D-π-D-A(Semiconductor) anchoring dyes to enhance the tunable NLO response: a DFT/TDDFT quest for new photovoltaic materials. Struct Chem. https://doi.org/10.1007/s11224-022-02070-3
35. Sumrra SH, Arshad Z, Zafar W et al (2022) Metal incorporated aminothiazole-derived compounds: synthesis, density function

theory analysis, in vitro antibacterial and antioxidant evaluation. R Soc Open Sci 8:210910. https://doi.org/10.1098/rsos.210910
36. Hassan AU, Mohyuddin A, Nadeem S et al (2022) Structural and electronic (absorption and fluorescence) properties of a stable triplet diphenylcarbene: a DFT study. J Fluoresc 32:1629–1638. https://doi.org/10.1007/s10895-022-02969-4
37. Hassan AU, Guleryuz C (2021) Theoretical evaluation of the permeability of the discharge item (LiOOH) in Li-O-2 batteries. Lat Am Appl Res 51:153–157. https://doi.org/10.52292/j.laar.2021.595
38. Glendening ED, Landis CR, Weinhold F (2012) Natural bond orbital methods. Wiley Interdiscip Rev Comput Mol Sci 2:1–42. https://doi.org/10.1002/wcms.51
39. Hassan AU, Sumrra SH, Zafar MN et al (2022) New organosulfur metallic compounds as potent drugs: synthesis, molecular modeling, spectral, antimicrobial, drug likeness and DFT analysis. Mol Divers 26:51–72. https://doi.org/10.1007/s11030-020-10157-4
40. Hassan AU, Sumrra SH, Nazar MF, Güleryüz C (2022) A DFT study on new photovoltaic dyes to investigate their NLO tuning at near infrared region (NIR) as pull–push effect by end capped acceptors. J Fluoresc. https://doi.org/10.1007/s10895-022-03075-1
41. Roch LM, Baldridge KK (2017) General optimization procedure towards the design of a new family of minimal parameter spin-component-scaled double-hybrid density functional theory. Phys Chem Chem Phys 19:26191–26200. https://doi.org/10.1039/c7cp04125j
42. Zou G, Ok KM (2020) Novel ultraviolet (UV) nonlinear optical (NLO) materials discovered by chemical substitution-oriented design. Chem Sci 11:5404–5409
43. Noreen S, Sumrra SH (2022) Correlating the charge transfer efficiency of metallic sulfa-isatins to design efficient NLO materials with better drug designs. Biometals. https://doi.org/10.1007/s10534-022-00385-6
44. Garmire E (2013) Nonlinear optics in daily life. Opt Express 21:30532–30544. https://doi.org/10.1364/OE.21.030532